# 1 Recoil-ion Momentum Spectroscopy and "Reaction Microscopes"

R. Moshammer, D. Fischer, and H. Kollmus

The rapid and still ongoing development of Recoil-Ion Momentum Spectroscopy (RIMS) during the last ten years can undoubtedly be viewed as an experimental break-through for the investigation of any kind of atomic reaction dynamics. Whenever atoms or simple molecules interact with electrons, ions or photons, the concept of high resolution recoil-ion measurements resulted in additional and complementary information compared to the traditional electron spectroscopy methods and in some cases even kinematically complete data sets, could be collected for the very first time. State of the art high-resolution recoil-ion momentum spectrometers evolved through numerous technical developments like, e.g., the implementation of cold supersonic-jet targets, the use of well defined electric extraction fields for recoil-ions as well as for electrons and the rapid progress in charged particle detection techniques. Among them the use of supersonic jets to produce well localized and internally cold targets (COLd Target Recoil-Ion Momentum Spectroscopy COLTRIMS) can be viewed as the most important ingredient. They allowed one to achieve a recoil-ion momentum resolution far below 1 a.u. (atomic unit) which would be impossible with room-temperature targets due to the thermal motion (the momentum spread of room-temperature helium atoms is about 3.7 a.u.). Another decisive development was the invention of completely novel and extremely efficient electron imaging concepts. In combination with COLTRIMS they enabled the detection of recoil-ions and electrons in coincidence and opened up a whole area of kinematically complete atomic reaction studies.

In this Chapter, we discuss the working principle of these modern spectrometers and try to give some advises for construction. We briefly discuss their range of applications but we leave out a detailed historical overview (for this the reader is referred to [1–3]). Our aim is to introduce the reader to the basics of COLTRIMS and Reaction Microscopes.

### 1.0.1 Imaging Spectrometers for Ions

A recoil-ion momentum spectrometer is a high precision device designed to measure recoil-momenta corresponding to kinetic energies in the order of a few meV with $\mu$eV resolution. In general, the recoil-ion momentum range of interest depends on the reaction channel to be studied. For example, in photoionization at photon energies just above the ionization threshold the recoil momentum will be extremely small, which essentially reflects the ejected

electron momentum. In violent collisions with highly charged ions or when Coulomb explosion of molecules is being studied, the ionic target fragments sometimes achieve kinetic energies in the eV range. From most atomic reactions, however, the created target ions emerge with typical momenta of 1 a.u. or lower (one atomic unit in momentum is the mean translational momentum of an electron bound in the ground state of a hydrogen atom). This corresponds to a kinetic energy of only 1.8 meV for a helium target.

In order to measure the magnitude and the direction of the recoil-ion momentum vector, an experimental arrangement is needed which performs an unambiguous mapping of these quantities onto experimentally accessible observables. One might think of using energy or momentum dispersive spectrometers like those extensively used in traditional electron spectroscopy. But, in spite of their excellent resolution, they suffer from transmission efficiency and, thus, they are inadequate for coincidence measurements. The most simplest device to fulfill the requirements of sufficient momentum resolution and large angular and momentum acceptance would be a position sensitive detector placed at some distance in a field free environment viewing the point like reaction volume. Then, simply from the position and time-of-flight (TOF) information of each detected ion, the trajectory can be reconstructed and the initial momentum vector can be calculated. The TOF has to be measured with respect to a trigger signal which uniquely defines the time of interaction of a projectile with a single target atom. To do so either a pulsed beam of projectiles (synchrotron radiation, pulsed lasers, bunched electron or ion beams) has to be used or single projectiles of a continuous beam have to be detected with a time sensitive detector, e.g., after the collision. In fact, spectrometers of this type have been applied in the pioneer-era of recoil-ion momentum spectroscopy [4]. But, this simple projection technique has some unacceptable drawbacks. The recoil-ion angular acceptance is limited and no direct information about the ionic charge is obtained. Moreover, unavoidable contact potentials can cause major problems. These difficulties are largely circumvented by applying a constant and weak homogeneous electric field to push the ions towards the detector [5]. This way, the angular and momentum acceptance is considerably increased and as long as the voltages applied at the spectrometer are much larger than typical contact potentials their influence and that of external stray fields is very weak. A further very important advantage is that with field extraction the TOF yields information not only about the ion momentum but in addition it allows one to determine the ion species because the TOF depends also on the ratio of ion mass over charge. In conclusion, a standard RIMS-Spectrometer consists of a region with a homogeneous electric extraction field where recoil ions emerging from an ideally point like source volume are accelerated. Afterwards they pass a field-free drift region for reasons which will be discussed later, before they are detected by means of a position sensitive ion-detector.

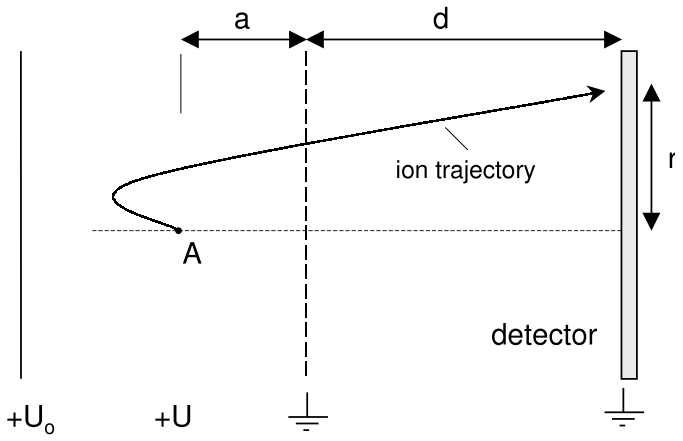


**Fig. 1.1.** Schematics of a recoil-ion momentum spectrometer.

To discuss the working principle in more detail let, us consider a recoil-spectrometer as shown schematically in Fig. 1.1. Let us assume that at the position A target atoms of mass $M$ are ionized due to any type of atomic reaction. During this interaction they acquire a small initial kinetic energy of $E_{\|} = P_{\|}^2/(2M)$, where $E_{\|}$ and $P_{\|}$ are the ion energy and momentum, respectively, along the spectrometer axis. This is the quantity we aim to measure. To extract the ions in a defined way a homogeneous electric field is superimposed to the reaction zone by applying for example a potential between a conductive back-plate and a grid or mesh. The resulting effective potential between the source point A and the grid is assumed to be $U$. Due to acceleration in the field the recoil-ions gain an additional kinetic energy of $qU$, where $q$ is the ion charge, before they pass through the grid. After traveling through a drift region (length $d$) they are registered in a position-sensitive detector. The recoil-ion time-of-flight as a function of their small initial energy $E_{\|}$ along the spectrometer axis and is given by

$$t_{+/-}(E_{\|}) = f \cdot \sqrt{M} \cdot \left[ \frac{2a}{\sqrt{E_{\|} + qU} \pm \sqrt{E_{\|}}} + \frac{d}{\sqrt{E_{\|} + qU}} \right], \qquad (1.1)$$

where the "+"sign stands for those ions which are emitted in the forward direction, i.e. toward the detector and the "−"sign for those with an initial backward velocity. Eq. (1.1) yields the TOF in ns, where the ion mass $M$ is expressed in amu (atomic mass units 1 amu $= \frac{1}{12}C_6^{12}$), distances in cm, energies in eV and the factor $f = 719.7 \cdot \sqrt{eV \cdot ns/cm}$ results from the conversion of units. The two terms in Eq. (1.1) correspond to the time the ions spend in the acceleration and drift region, respectively.

Usually the extraction potential $qU$ is much larger than $E_{\|}$ and therefore different ion species and/or charge states appear as well separated peaks in

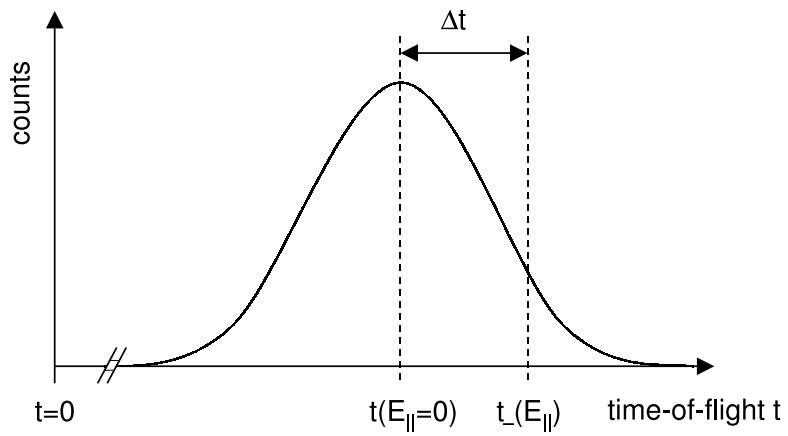


**Fig. 1.2.** Schematic recoil-ion time-of-flight distribution (TOF-peak).

the TOF-spectrum. Then, and if recoil-ions emerge with equal probability in the forward and backward direction, the position of the corresponding peak is given by

$$t_0 = t(E_{\|} = 0) = f\sqrt{M/qU} \cdot (2a + d) \tag{1.2}$$

and its shape reflects the initial energy or momentum distribution, respectively. This is true as long as $qU >> E_{\|}$. In this case a linear expansion of $t(E_{\|})$ (Eq. (1.1)) around $t_0$ can be used to determine the initial energy. For large initial kinetic energies, i.e. when $E_{\|}$ becomes comparable to $qU$, this approximation can cause unacceptable distortions. This happens most likely when energetic ions from molecular Coulomb-explosion or electrons are imaged. In this case Eq. (1.1) has to be solved numerically to extract $E_{\|}$ as a function of time. For all atomic reactions, however, where slow ions emerge, it can be easily shown that those arriving with an time offset $\Delta t$ with respect to $t_0$ had an initial kinetic energy of

$$E_{\|} = \frac{1}{4M} \cdot \left(\frac{U \cdot \Delta t}{a \cdot f}\right)^2 . \tag{1.3}$$

This follows directly from solving $2\Delta t = (t_-(E_{\|}) - t_+(E_{\|}))$ using Eq. (1.1). With Eq. (1.3) it is possible to assign to each channel in the TOF-spectrum the corresponding recoil-ion momentum ($P$ in a.u., $qU$ in eV, $a$ in cm and $\Delta t$ in ns)

$$P_{\|} = 8.042 \cdot 10^{-3} \cdot \frac{qU}{a \cdot \Delta t} . \tag{1.4}$$

For flight times shorter than $t_0$ the initial ion velocity vector was pointing towards the detector and vice versa. Interestingly, this relation is independent

on the particle mass, it is valid for ions as well as electrons. Moreover, only the knowledge about the electric field strength $U/a$ at the source point is required to calculate the momentum component along the spectrometer axis and no further information about the overall geometry of the spectrometer is needed. Thus, with a time-resolution of 1 ns in the TOF measurement under otherwise ideal conditions, a momentum-resolution below 0.01 a.u. is achievable when a field of 1 V/cm is used for extraction.

### 1.0.2 Time Focusing

The above discussion is based on the assumption of a point like source volume. This is fairly unrealistic. A extended reaction zone over a certain width $\Delta a$ has two consequences. First, the ions start at different potentials and second, they travel over different acceleration distances $a + \Delta a$. According to Eq. (1.1) both effects give rise to an effective time jitter $\delta t$ as a result of the target extension of

$$\frac{\delta t}{t} = \frac{2a - d}{4a + d} \cdot \frac{\Delta a}{a} . \tag{1.5}$$

Thus, for a spectrometer without drift ($d = 0$) where $He^+$ ions are extracted by a filed of 1 V/cm, a source volume size of only 1 mm results in a time jitter of about 45 ns. According to Eq. (1.4) this corresponds to a momentum uncertainty of more than 0.3 a.u., demonstrating that a device with pure extraction only is inappropriate for momentum spectroscopy. On the other hand, if a drift path with a length of $d = 2a$ is introduced then the influence of the target size can be eliminated completely (Eq. (1.5)), at least in the first order. This is the so-called *time-focusing condition* for spectrometers with one acceleration and one drift region [6].

A similar condition can be found for other combinations of several acceleration and drift regions. A further conclusion arises from Eq. (1.5), namely that the influence of the source volume extension on the momentum resolution is reduced if the geometrical size of the spectrometer is increased. This is not surprising, but it should be taken into account in the design of time-of-flight spectrometers. In the construction of spectrometers it is worth to spent efforts in order to really fulfill the time-focusing condition. If the drift path of our example spectrometer (10 V extraction over 10 cm plus 20 cm drift) would be too short by only 1 cm then the momentum resolution would be limited to be not better than 0.025 a.u.. Even stronger influence has a not well adapted acceleration distance which is sometimes hard to determine experimentally. It requires an exact knowledge of the location where the projectile beam interacts with the target-gas beam. Spectrometers with more than one acceleration region represent an alternative because they allow one to adjust the time-focusing condition via the applied voltages even for unknown or shifted target positions.

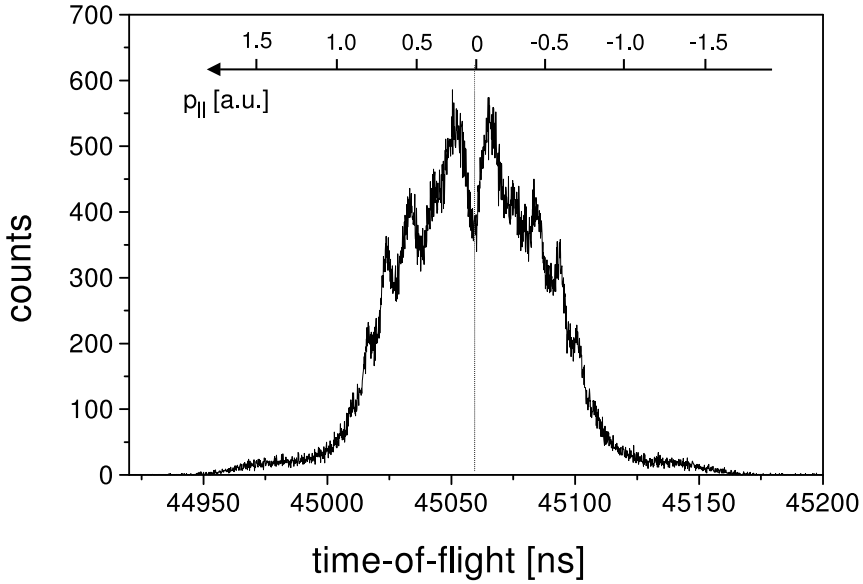


**Fig. 1.3.** TOF-distribution of $Ar^+$ ions for single ionization with strong 25 fs laser-pulses (at a light intensity in the upper $10^{13}$ W/cm$^2$ range). The laser polarization direction is parallel to the TOF-axis. The appearance of individual peaks reflects the absorption of single 1.5 eV photons above the ionization threshold.

### 1.0.3 Reconstruction of Momentum Components

The recoil-ion longitudinal momentum, i.e. the component along the electric field axis, is unambiguously related with its time-of-flight. An example is shown in Fig. 1.3 for ionization of Ar in intense laser fields. The ions were extracted with a field of 1 V/cm using a spectrometer with time focusing. In this specific case the $Ar^+$ ion has to balance the momentum of the ionized electron. This follows from momentum conservation for a negligibly small momentum carried by the absorbed photons. The result of the conversion from TOF into $P_{||}$ is shown in the inset of Fig. 1.3 demonstrating that structures in the order of 0.1 a.u. are clearly resolved. This corresponds to a kinetic energy of only 1.8 $\mu$eV. The two missing momentum components perpendicular to the field vector can be determined from the position of impact on the ion detector. Thus, all three components of the recoil-ion momentum vector are determined by a coincident measurement of the two position coordinates and the time-of-flight for each ion.

In the following the reconstruction of the transverse momentum $P_\perp$ will be discussed. For simplicity we first assume again a point like source and try to calculate the trajectory of an ion which is emitted in an arbitrary direction with an energy $E$. To stay with our notation we split this energy into two

parts, $E_\parallel$ and $E_\perp$, where $E_\perp = P_\perp^2/(2M)$ is the initial kinetic energy in the direction perpendicular to the electric field vector. Ions with $E_\perp = 0$ would hit the detector exactly in the center while in general they are registered with a certain displacement $r$ (see Fig. 1.1) which is given by

$$r = \frac{1}{f} \cdot \frac{\sqrt{E_\perp}}{\sqrt{M}} \cdot t(E_\parallel)\,, \tag{1.6}$$

where $m$ is given in amu, $E$ in eV and $t$ in ns, $r$ in cm. The radial deflection $r$ at the detector depends on both, the transverse and the longitudinal momentum, resulting in a very bulky expression if Eq. (1.1) would be inserted. A considerable simplification is achieved if the mean flight-time $t(E_\parallel = 0)$ of the specific ion is inserted instead of $t(E_\parallel)$. This approximation is very well justified as long as the width $\Delta t$ of the ion TOF-peak is much smaller than the mean flight-time or, in other words, as long as the kinetic energy gained due to the extraction is significantly larger than the initial recoil-ion energy. With Eq. (1.2) we get

$$r = (2a + d) \cdot \sqrt{\frac{E_\perp}{qU}}\,. \tag{1.7}$$

From this it follows immediately ($P$ being in a.u., $M$ in amu, $qU$ in eV and distances in cm)

$$P_\perp = 11.6 \cdot \frac{r}{(2a + d)} \cdot \sqrt{qU \cdot M}\,. \tag{1.8}$$

Hence, from the two spatial coordinates measured with the position sensitive detector the recoil-ion momentum components in the plane of the detector surface are obtained. Together with the TOF-information the full ion momentum vector can be reconstructed.

The achievable momentum resolution depends on the position resolution $\Delta r$ of the detector and, for more realistic situations, on the extension of the target zone. In many situations the latter is dominating. For our example spectrometer with time-focusing geometry and 10 eV extraction over $a$ =10 cm a target extension of $\Delta r$ = 1 mm causes a transverse momentum uncertainty of $\Delta P_\perp = 0.18$ a.u. for He ions. Keeping the concept of an homogeneous extraction field, the resolution can be improved only at the expense of a reduced transverse momentum acceptance either by lowering the applied voltage or by increasing the spectrometer size.

### 1.0.4 Spectrometers with Position Focusing

To circumvent the problem of limited resolution due to the reaction volume extension, which is in the mm-range even if well collimated supersonic gas-jet targets are used, spectrometers with the so called position-focusing have been developed [7,8]. They focus ions starting at different positions onto a

single spot on the detector while the displacement on the detector is still proportional to the initial momentum. Thus, the resolution is not limited by the source extension but by the imaging properties of the spectrometer. To achieve position focusing, a weak electrostatic lens is implemented into the acceleration region, preferentially as close as possible to the reaction zone. Using a stack of ring electrodes to generate the extraction field, either a homogeneous or a lensing field can be realized by applying appropriate potentials to the electrodes. However, the implementation of a lens in the extraction region modifies the focusing properties in the third, the time-of-flight direction. To obtain both, position and time focusing, a longer drift tube compared to spectrometers with homogeneous extraction is required. A proper tuning of spectrometer geometry and field parameters is necessary to accomplish that the focal points for the time-of-flight and for the spatial focusing coincide exactly at the detector. Spectrometers with position focusing have been used mainly to study electron capture reactions in ion-atom collisions where the recoiling target ions acquire different but discrete momenta parallel to the beam direction corresponding to different final electronic states of the captured electron [8]. To resolve these lines in the momentum spectrum a high resolution is decisive.

### 1.0.5 Electric Field Distortions and Calibration

Besides the source volume extension and the finite position and time resolution, otherwise idealized conditions have been assumed up to this point. In real spectrometers distortions due to electric stray and fringe fields, contact potentials, imperfect geometry and external magnetic fields have to be considered. Unavoidable and sometimes severe distortions are produced when grids with large gap widths are used to separate the extraction part from the drift region. The openings of the grid act as individual lenses and even small deflections of passing ions can result in magnified images of the grid structure at the detector destroying the unique assignment of ion momentum and position of detection. Moreover, field penetration through grids into e.g. the field-free drift tube can cause a significant change of the spectrometer imaging properties and a break down of the time-focusing condition. This is hardly avoidable because after the drift part a region of very high field strength is required to post-accelerate the ions up to several keV in front the detector in order to achieve a reasonable detection efficiency. Depending on the gap width of the grid used to shield the drift part from the post-acceleration region a more or less prolonged drift path is required to compensate the effect of field penetration. Grids with small gaps are in favor but, on the other hand, very fine grids suffer from low open areas and therefore reduce the ion transmission. Grids with a wire spacing between 50 to 250 $\mu$m represent a reasonable compromise. In any case, due to the lensing effect the wire spacing represents an upper limit of the achievable position resolution of the detector.

In some situations it is not trivial to assign the point of zero transverse momentum to a certain position coordinate on the detector. One can either calibrate the spectrometer with well known reactions, like electron capture, or one chooses a orientation of the spectrometer in such a way that the extraction is parallel to a symmetry axis of the physical process to be studied. In the latter case, the center of gravity of the ion position distribution corresponds to zero momentum. Possible outstanding axis of atomic reactions are the polarization direction in photoionization or the beam axis for charged particle impact. In general, it is advantageous to make use of these symmetries, because it facilitates to interpret and sometimes to cross check the experimental data. After having determined the zero point the spectra have to be calibrated.

This can be done by several ways. In particular, spectrometers with position focusing have to be calibrated either by relying on calculated calibrations (using, e.g., the SIMION program) or via capture measurements. In most cases, and in particular for well known spectrometer geometries and when homogeneous fields are used, it is precise enough (within a few percent) to apply the calculated dependence of initial momentum and position for calibration.

### 1.0.6 Target Preparation

A prerequisite for high resolution recoil-ion momentum spectrometry is a cold atomic or molecular gas-target because in many cases, depending on the physical process to be studied, the recoil-ion momenta are of the order or even smaller than the thermal momentum spread at room temperature. Moreover, and as already discussed, a small target size is indispensable for momentum spectroscopy with imaging spectrometers. In almost all existing devices both requirements are realized with supersonic expansion of the target gas to form a well localized cold atomic beam.

### 1.0.7 Supersonic Jets

When a gas is pressed through a small nozzle into a reservoir at low pressure it is accelerated to supersonic speed at the exit of the nozzle and an atomic beam is formed as long as the pressure ratio is larger than about two (for more detailed information see [9]). During this adiabatic expansion the free enthalpy $H = 5/2 k_B T_0$ ($k_B$ being the Boltzmann constant and $T_0$ the gas temperature before expansion) of an ideal gas is converted into a directed motion at the expense of the internal temperature. Under ideal conditions no internal atomic motion is left over in a frame where the atoms (with mass $M$) move with a momentum of

$$p_{jet} = \sqrt{5 k_B T_0 M}\,. \tag{1.9}$$

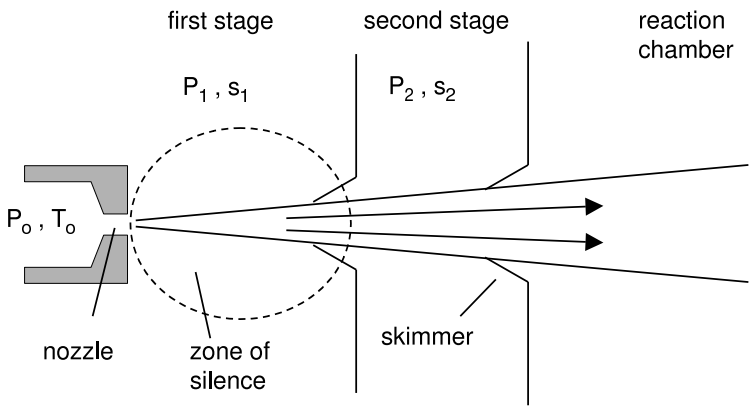


**Fig. 1.4.** Schematic representation of a two-stage supersonic gas jet.

For a helium gas at room temperature we get $P_{jet} = 5.9$ a.u. corresponding to a translational kinetic energy of 65 meV. In practice these ideal values are not reachable but some internal temperature is left in the gas jet. This is expressed by the speed ratio $S$, i.e. the ratio of the translational jet-velocity to the thermal velocity-spread

$$S = \sqrt{\frac{5T_0}{2T}}\,, \tag{1.10}$$

where $T$ is the internal temperature after expansion. The speed ratio depends on the gas species, the gas temperature and on the product of the driving pressure and the nozzle diameter $p_0 \cdot d$.

Reasonable gas-jet properties are obtained for $p_0 \cdot d > 1$ torr·cm. Below this value the regime of supersonic flow behind the nozzle extends over a distance of only a few nozzle diameters, which is usually not sufficient to extract a supersonic beam. For $p_0 \cdot d > 10$ torr·cm clustering effects are certainly a concern for pure gases at room temperature. In this respect helium is an exception and much higher driving pressures can be applied resulting in large speed-ratios or low internal jet-temperatures, respectively. To produce a helium gas-jet with a speed-ratio of $S = 50$, corresponding to an internal jet temperature of $T = 0.3$ K, by expanding the gas at $T_0 = 300$ K through a 30 $\mu$m diameter nozzle a driving pressure of about 25 bar is required. Under similar conditions but with pre-cooling of the gas before expansion the jet velocity is reduced and considerably larger $S$-values can be obtained. In practice, however, the achievable jet-performance is mainly limited by the pumping speed in the first stage. One or several stages with differential pumping are used to handle the enormous gas-load and to maintain a good vacuum in the reaction chamber. To extract a geometrically well defined supersonic beam a small "skimmer" aperture is placed behind the nozzle and

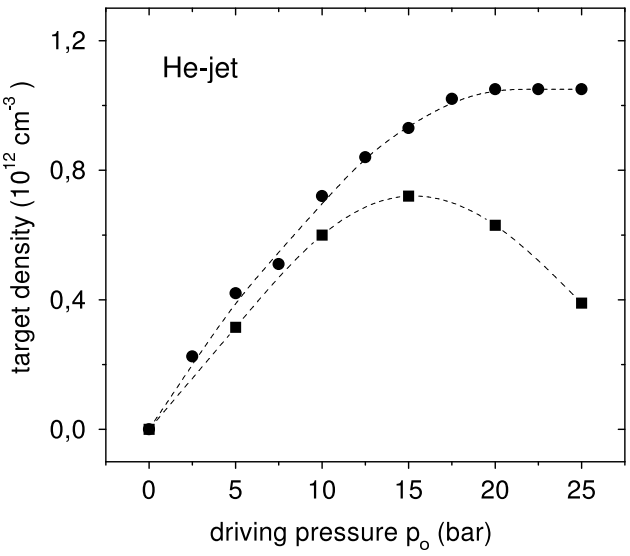


**Fig. 1.5.** Density of a He gas-jet for a pumping speed of 500 l/s (circles) and 250 l/s (squares) in the first stage. The nozzle diameter is 30 $\mu$m.

between the different pumping stages (Fig. 1.4). The most critical values in the design of a gas jet are the pumping speed in the first stage and the nozzle-skimmer distance. At the nozzle exit a zone of supersonic flow bordered by a compression or shock-front is formed. A high quality gas-jet can be cut out if the edge of the skimmer immerses into this so-called "zone of silence", which typically extends over a range of several mm up to cm strongly depending on the background gas pressure $p_1$ in the first stage. The performance is quite insensitive to the nozzle-skimmer distance and to the skimmer shape as long as a high vacuum of $p_1 < 10^{-3}$ torr is maintained. To achieve this, however, huge pumps are required. For our He-jet example either a 10000 liter/s pump would be needed or the driving pressure has to be reduced equivalently resulting in a lower speed-ratio and lower beam intensity. The pressure rise (in torr) in the first stage can be estimated from the balance of pumping speed $s_1$ (in liter/s) and gas-throughput by

$$s_1 \cdot p_1 = C \cdot \left(\frac{300}{T_0}\right)^{3/2} \cdot p_0 \cdot d^2 \,, \tag{1.11}$$

where $C$ (in liter/cm$^2$/s) is a gas dependent factor ranging from about $C = 10$ for heavy gases up to C $\approx 50$ for He and molecular hydrogen. Accordingly, a background pressures in the $10^{-2}$ torr range is achievable with a modern 500 liter/s turbo-pump. In this case, the zone-of-silence typically extends

only over a few mm and the skimmer shape and in particular the nozzle-skimmer distance becomes decisive. At lower pumping speeds, and therefore higher background pressures, the zone-of-silence extension is reduced further. But, only if the skimmer tip dives into the zone of silence a well defined and cold supersonic beam can be extracted. The influence of the pumping speed on the jet density is demonstrated in Fig. 1.5. The gas density at the target position, i.e. 10 cm downstream from the nozzle, was measured as a function of the He driving pressure for different pumping speeds but with a fixed nozzle- skimmer distance [10]. The latter was optimized for the 500 liter/s pump. The degrading of the jet performance at high pressures with the smaller pump could have been avoided by reducing the nozzle-skimmer distance slightly. Therefore, the possibility to easily adjust the nozzle position should be foreseen in the construction of a jet device in order to obtain the best performance for different gas species and driving pressures.

For most applications a dense and narrow atomic beam is required which is crossed with a projectile beam in the interaction chamber. Without to much effort supersonic gas beams with a particle density in the order of $10^{11}$ to $10^{12}$ $cm^{-3}$ at a distance of about 10 cm away from the nozzle are reachable. It is obvious, that this number decreases with the inverse square of the distance between the nozzle and the interaction zone. What finally determines the event-rate in crossed-beams experiments is the target-area density. It increases with the geometrical size of the gas beam. The latter is defined by the nozzle-skimmer geometry, i.e. the skimmer orifice and the nozzle-skimmer distance. A small interaction volume, which is given by the overlap between the projectile and target beam, can be obtained with narrow gas beams resulting in a high momentum resolution in combination with RIM spectroscopy. If event rate is a concern, it might be necessary to work with broader gas-beams in combination with a time and position-focusing recoil-spectrometer to maintain a good recoil-ion momentum resolution. Though supersonic expansion reduces the target temperature by up to a factor of 1000, or even more if pre-cooling is used, the remnant target momentum spread certainly sets a lower limit in the achievable ion momentum resolution. In the direction parallel to the gas-jet velocity the momentum spread is given by the intrinsic jet-temperature. For a helium jet with a speed-ratio of $S = 50$ starting at room-temperature this momentum uncertainty is about 0.13 a.u.. The perpendicular momentum spread is much smaller, it is determined by the jet velocity and the divergence of the atomic beam. If one or several skimmers are used to cut out a He-jet which has a diameter of 1 mm at a distance 10 cm away from the nozzle then this momentum spread is below 0.06 a.u.

Over the last five years supersonic gas-jets became the standard devices to produce cold and localized atomic or molecular targets in connection with recoil-ion momentum spectroscopy (COLTRIMS). With this method a large variety of different gases is accessible ranging from helium or other noble

gases up to any type of molecular gases. Cooling of the gas before expansion is useful for helium or molecular hydrogen to reduce the internal gas-jet temperature and to reach the optimum momentum resolution but it can lead to the formation of clusters or liquid droplets if heavy gases are used. One should also be aware that the internal momentum spread increases with the mass $m$ of the gas even if the same final jet temperature is obtained. Thus, the generation of a gas jet with a low intrinsic momentum spread of $\Delta P <$ 0.5 a.u. along the jet-direction is definitely hard to achieve for gases heavier than argon.

### 1.0.8 Atomic traps (MOTRIMS)

A significantly further reduction of the target temperature is achievable when laser-cooled atoms trapped in an Magneto-Optical-Trap (MOT) are used as a target. In the first pioneering experiment, Wolf and Helm [11] have measured recoil-ion energies of photoionized Rb atoms extracted from a MOT with very high resolution. Basically the same method has been used very recently [12–14] to study single electron capture reactions in keV ion collisions with atoms trapped in a MOT. In these first experiments a unprecedented resolution in the recoil-ion momentum has been achieved by taking benefit from the sub-mK intrinsic temperature of the target. For recoiling $Rb^+$ ions produced in capture reactions with keV $Cs^+$ projectiles Flechard and coworkers [14] have obtained a momentum resolution of $\Delta P = 0.03$ a.u., which means that the recoil-ion velocity has been measured with a sensitivity of below 1 m/s. Certainly, this value is not the ultimate resolution set by the gas cloud temperature of typically 100 $\mu$K. It would correspond to a momentum resolution of $\Delta P = 0.003$ a.u. for lithium and $\Delta P = 0.01$ a.u. for rubidium.

With typical densities in the range of several $10^{10}$ cm$^{-3}$ and radii of 1mm or below, the atomic clouds trapped in MOT are ideally suited as targets for RIMS (MOTRIMS). Whenever an ultimate momentum resolution is desirable like, e.g., in electron capture reactions where the recoil-ion momentum gives direct access to the electronic sates populated in the projectile ion, a MOT target is superior to any gas jet. Another important aspect is, that the palette of possible targets for RIMS is considerably widened. All alkali and earth alkaline atoms are easily trapped in a MOT, but they are hardly produced and cooled in a supersonic gas jet. These atoms are in some situations of particular interest because they represent single active electron targets and therefore have many features in common with atomic hydrogen, the simplest atomic target which is not directly accessible to COLTRIMS because efficient cooling methods are not at hand. Besides, other interesting options are laser excited atoms and the possibility to probe the occupation of these excited states in a time-resolved manner via capture reactions [15] monitored with RIMS.

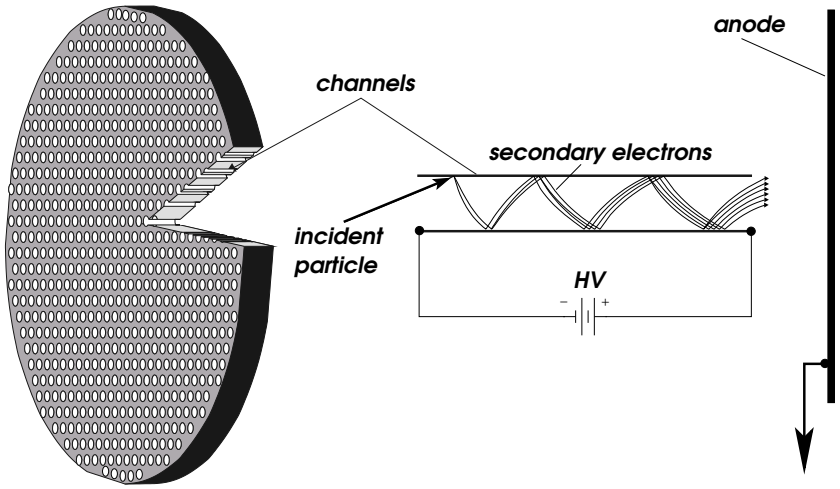


**Fig. 1.6.** Working principle of a channel-plate detector.

### 1.0.9 Position Sensitive Detectors

For recoil-ion momentum spectroscopy large-area position-sensitive detectors with good position resolution (typically 0.1 mm or better) and fast timing signals (below 1 ns) are essential. Multi-Channel-Plate (MCP) detectors with either chevron (two plates) or z-stack (three plates) configuration and typical plate diameters of 50, 80, or 120 mm are used. They have a typical detection efficiency for charged particles of about 60 % mainly determined by the open area. This optimum efficiency is obtained for ions that hit the detector-surface with a kinetic energy of about 2 keV or more and for detection of electrons the efficiency is best at energies between 100 and 300 eV. For position encoding the emerging electron cloud created by avalanche amplification in the MCP-channels is analyzed by means of wedge & strip [16] or delay-line anodes [17] at the backside of the detector.

### 1.0.10 Wedge & Strip Anodes

The working principle of a position-sensitive detector with a wedge & strip anode is the following. The amplified electron cloud, containing about $10^5$ - $10^6$ electrons, is accelerated onto a segmented anode consisting of electrically separated areas with a wedge & strip structure at a typical periodicity of 1.5 mm (Fig. 1.7). Since the area of the wedges and the stripes depends linearly on the $x$ and $y$-position, respectively, the pulse heights of the signals picked up at both electrodes are proportional to the position of the cloud centroid, as long as the cloud covers an area larger than one period of the anode structure. This is ensured by letting the electrons expand during their travel over a distance of several mm from the MCP to the anode. In a more refined

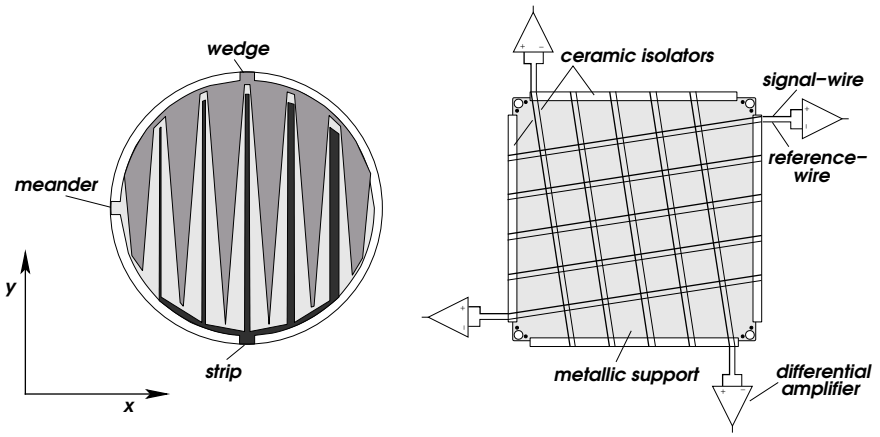


**Fig. 1.7.** Left: Structure of a wedge & strip anode with a strongly reduced number of periods to illustrate the $x$ and $y$-dependence of the electrically separated areas. Right: Two cable-pairs wrapped in multiple turns around a metallic support form a delay-line anode. With ceramic holders the electrical isolation between cables and support and among the cables is ensured.

anode-concept, the wedge & strip structure is evaporated onto the backside of a glass-plate. The front-side is covered with a thin Ge-layer which collects the electron cloud [18]. In this case the segments pick up the image charge of the Ge-layer while the widening of this image charge is adjusted by a proper selection for the Ge-layer resistivity and the thickness of the glass-plate. This concept has the advantage that the detector can be operated in strong magnetic field environments. In any case, to extract the position information the pulse heights of the wedge and stripe segments have to be normalized to the collected total charge, which varies from event to event. It is given by the pulse height sum of all electrodes, the wedge, the strip and a meander structure which fills the area between the first two. All three signals are amplified in separate charge-sensitive preamplifiers and subsequent spectroscopy amplifiers and recorded by analog-to-digital converters. The event-by-event normalization and calibration procedure is usually done by software. The position information is obtained from the measured pulse heights reflecting the amount of charge collected by the wedges $Q_W$, the stripes $Q_S$ and the meander $Q_M$, respectively

$$X \propto \frac{Q_S}{Q_S + Q_W + Q_M} \quad , \quad Y \propto \frac{Q_W}{Q_S + Q_W + Q_M} \, . \tag{1.12}$$

For a correct imaging, the amplifiers in the individual channels have to be adjusted properly and if great demands are put on linearity then the capacitive cross-talk between the electrodes has to be considered. This correction can be done by software. In addition, a high gain of the MCP detector is important for a good position resolution because the main limiting factor is

the signal-to-noise ratio of the signals. With standard amplifiers a position resolution of 0.1 mm or better is easily achievable for a 50 mm diameter anode. For timing purposes a fast signal can be picked up either at the front or at the back side of the MCP-stack and a time resolution well below 1 ns is easily achievable. Since several $\mu$s are required for signal integration and pulse shaping the maximum count-rate is limited to about 100 kHz.

### 1.0.11 Delay-Line Anodes

The position readout with a delay-line anode combines both, high count-rate capabilities and good position resolution. In this case the position encoding is done by a measurement of the time a signal needs to travel along a wire which is wound in many loops around a rectangular support with a wire spacing in the order of 0.5 mm [17]. The time difference between the signals arriving at both ends of the wire is proportional to the position coordinate where the charge cloud has been collected (Fig. 1.7). The finally achievable position resolution is not limited by the wire spacing because, similar to wedge & strip anodes, a cloud centroid averaging occurs also with delay-line anodes. For the second spatial coordinate another wire is wound perpendicular to the first one. In practice, a pair of wires forming a Lecher-cable is used for each direction. Since both wires of the Lecher-cable pick up a completely identical noise via capacitive coupling with the surrounding their signals differ only if a real charge is deposited on one but not on the other wire. To ensure that only one wire collects the electrons from the cloud it is biased with a more positive potential and the second one is basically used to monitor the noise. The ends of the Lecher-cables are fed into fast differential amplifiers to subtract the noise from the signal and to enable a precise determination of the time difference between both ends of the Lecher-cable. Fast discriminators and Time-to-Digital Converters (TDC) are used for further signal processing and read-out. From the collected timing information the $x$ and $y$-coordinates can be calculated by

$$X = (t_{x1} - t_{x2}) \cdot v_{signal} \quad Y = (t_{y1} - t_{y2}) \cdot v_{signal}\,, \tag{1.13}$$

where $(t_{x1} - t_{x2})$ is the time difference between the signals arriving at both ends of the wire wound in $x$-direction. The differenz $(t_{y1} - t_{y2})$ is the corresponding value for the $y$-direction. Though the signals travel almost with the speed of light along the wire the essential signal velocity $v_{signal}$ is much smaller. It is determined by the time a signal needs to pass the anode from one side to the other which is about 70 ns for a delay-line anode of 80 mm square. The position resolution is related to the precision obtained for the determination of the time difference between the signals collected at both ends of the delay-line wire. It can be measured very accurately and position resolutions of 0.1 mm are routinely achieved with delay-line anodes [19]. According to Eq. (1.13) a time zero or the absolute time of arrival of a particle

on the detector is not needed to extract the position information. Usually the absolute time is defined by the timing signal of the MCP-stack. With respect to this time base the time sums $(t_{x1} + t_{x2})$ and $(t_{y1} + t_{y2})$ are constant and equal to the transition time from end of the wire to the other. This additional information can be used for consistency checks or, as will be discussed afterwards, for multi-hit purposes.

### 1.0.12 Multiple Hit Detection

In most applications the delay-line concept is superior to position encoding based on charge division like, e.g., wedge & strip and resistive anodes, because of several reasons. In general the most important advantage is the very fast read-out allowing count-rates of several MHz limited mainly by the performance of the MCP and of the electronics. Another advantage is that large area delay-line anodes can be produced easily without loss of position resolution whereas a simple scaling up of a wedge & strip structure results in a proportional degrading of the absolute resolution. Only for very long wires the signal dispersion becomes a matter of concern. Regarding COLTRIMS and, in particular, electron momentum imaging, an essential advantage is the ability to register the time and position information of multiple hits, or showers of particles arriving at the detector within a very short time interval.

The relevant time scale is set by the total delay time of the anode wires, which is between 30 and 100 ns depending on the size of the detector. As long as the time separation between two subsequent hits is larger than this total delay, no particular arrangements are needed to record their position and time, except of an electronic device for handling several consecutive signals (like, e.g., a multi-stop TDC). In this case the five signals (4 from the anode plus one from the MCP) of the first particle arrive first and those of the second hit arrive always later. This mode of operation with a dead-time in the order of 50 ns enables already a large variety of experimental studies, like e.g. imaging of ionic fragments from molecular Coulomb-explosion where the number of accepted fragments is limited only by the performance of the TDC. But, the detector dead-time can be reduced much further if a more advanced signal assignment and data recovering is used. As already mentioned, the detector delivers five timing signals for each registered particle, but only three informations are needed to extract the position and the absolute time. It is basically this redundancy which allows to reconstruct the positions of a double or multiple-hit event where the time separation of consecutive hits is considerably shorter than the total delay time of the anode. In this case, if two particles hit the detector at very different positions, it may happen that some signals from the delay-line are not in the right order (a signal from the second particle may arrive first) or some may even be missing because of signal overlapping. Using the fact, that the time-sum of signals belonging together is constant and known, the correct signal ordering can be recovered and the corresponding particle positions can be determined. Moreover, if a signal is

completely missing the spatial positions are still accessible, because a signal on one end of the delay-line wire is sufficient to determine the corresponding coordinate. Only when the signals from both ends of one delay-line wire are missing the position information is lost. Using this scheme of reordering and data recovery, the actual detector dead-time is reduced to zero as long as the $x$- and $y$-coordinates of subsequent particles differ by more than the corresponding pulse-pair resolution of the detector system which is mainly limited by the signal widths and the pulse-pair resolution of the TDC. The latter is usually in the 5-10 ns range resulting in a crossed- shaped dead-zone of some mm width in the position difference of two subsequent hits.

Based on either a complete or partial reconstruction of delay-line signals several experiments have been performed for imaging of up to three electrons emerging from a single breakup of atoms or molecules in collisions with photons, electrons or ions. In these experiments, with typical electron flight-times of some 100 ns, the residual detector dead-time turned out to be not a severe limitation since in many cases the physics hinders electrons to arrive exactly at the same time at identical positions on the detector. Nevertheless, the left-over dead-time sometimes complicates the interpretation of experimental data because always a certain part of the electron kinematics is cut out. Thus, a detector concept without any restrictions concerning the multi-hit capability would be desirable.

Such a delay-line anode, having practically no dead-time at all, has been developed by Jagutzki and coworkers [20]. The basic idea is to further increase the number of redundant signals delivered by the anode. This has been achieved by taking three instead of two wire-pair layers and by winding them not perpendicular to each other but with an angle of 60 degree around a hexagonal shaped support. Thus, for each hit one signal from the MCP plus six from the anode are obtained whereas only three of them are needed for timing and position encoding. The additional signals can be used for cross-checks and data recovering. With this newly developed delay-line concept the dead-time is reduced further allowing to accept events where two particles hit the detector at the same time at almost identical positions without loss of information. It can be anticipated that the hexagonal anode will become the ideal tool for a large variety of applications where high demands are put on the multi-hit processing in combination with good position resolution at comparably low system complexity.

## 1.1 Imaging Spectrometers for Electrons: Reaction Microscopes

For most atomic reactions the detection of the target ion only yields not sufficient information to characterize the reaction completely. Whenever more than two particles emerge, the desire to obtain the kinematically complete information requests the determination of all momenta for all outgoing parti-

cles in coincidence and for each single event. To achieve this it is sufficient to measure the momentum vectors of all target fragments but not the projectile because the momentum transferred from the projectile to the target can be deduced using momentum conservation. This strategy has been applied in various charged particle-atom collision experiments (see [1–3]). The task is somewhat less demanding in the case of photon induced ionization reactions because there the photon is absorbed and simply not present in the final state. Therefore the complete reaction kinematics is obtained by registration of all charged fragments except of one. In general, however, one or several electrons plus at least one or even more ionic fragments are emitted which requires the detection of ions and electrons in coincidence with high efficiency covering a large range of the final state momentum space to obtain maximum information.

Combined recoil-ion electron momentum spectrometers have been developed within the last ten years which fulfill to a large extend these requirements and which enabled kinematically complete studies of atomic collision reactions with up to five outgoing particles, e.g., triple ionization of Ne in collisions with heavy ions [21]. For the majority of atomic break-up reactions the assumption holds that electrons and ions emerge with momenta of comparable magnitude. Therefore, as a result of the ion to electron mass ratio, the kinetic energies of electrons exceeds those of typical recoil-ions by many orders (they are in the eV-range) making it much harder to collect electrons with high efficiency. The radial displacement on the detector scales with the square-root of the kinetic energy (Eq. (1.7)). Basically two concepts have been developed to achieve a high acceptance together with a good resolution for both, electrons and ions, in coincidence. Both approaches have in common that particle imaging is done by accelerating electrons and ions in the same electric field into opposite directions onto two position sensitive detectors. Because only the low energy part of the electron continuum is accessible with these devices another concept has been introduced taking advantage of the fact that in particular the electron trajectories are easily modified by small magnetic fields. With proper combined electric and magnetic fields the motion is effectively confined in space. This way extremely versatile spectrometers have been constructed, so called reaction-microscopes, allowing to adjust the resolution and the acceptance in the electron and ion branch individually. Both approaches, direct imaging and magnetic guiding of electrons, will be discussed in the next sections.

### 1.1.1 Direct Imaging of Electrons

The conceptually most obvious scheme for coincident imaging of electrons and ions is to place a second position sensitive detector opposite to the ion detector. The homogeneous electric field pushes them onto their individual detectors. In this case the same equations as those for the ions can be applied to reconstruct the electron momentum vectors from their time-of-flight and

position of detection. However, because the initial electron energies easily approaches the kinetic energy they gain in the extraction field, no approximate equations should be used to calculate neither the longitudinal momentum from the measured TOF nor the transverse energy from the position information. In fact, the full Eq. (1.1) and (1.6) must be solved for $E_\perp$ and $E_\parallel$, respectively. The achievable resolution is, in analogy to the recoil-ion branch, limited mainly by the source extension, the detector position resolution and the precision of the TOF measurement. The finite target temperature, which considerably contributes to the ion resolution, does not impose an additional uncertainty on the electron momentum. It results only in a negligibly small electron momentum spread because of the large atom to electron mass ratio. As a consequence unprecedented energy resolutions for electrons are achievable. Using our example spectrometer with time-focusing geometry and 10 V extraction over 10 cm to image electrons emitted from an extended target ($\Delta r$ =1 mm), one can easily achieve an energy resolution as small as $\Delta E_\perp$ = 62 $\mu$eV for the transverse direction and $\Delta E_\parallel \approx 1.3$ meV in the TOF-direction (time resolution $\Delta t$ = 1 ns). But the accepted maximum electron energy in the transverse direction is in the order of only some ten meV (less than 100 meV for a 80 mm diameter detector). For many applications this is too small.

The acceptance can be increased considerably by placing the detector closer to the target zone and/or by increasing the extraction voltage. This leads to smaller electron flight times and, therefore, to a lower momentum resolution in the TOF-direction. Moreover, a direct consequence of an increased extraction field is a slightly reduced momentum resolution for the recoil-ions. Nevertheless, direct electron imaging in coincidence with recoil-spectroscopy is ideally suited to investigate atomic reactions where electrons with small or very small continuum energies are generated. Placing the electron detector very close to the reaction volume (in the order of 1-2 cm) allows to detect electrons with $4\pi$ solid angle for energies in the few eV range. Such spectrometers have been used to study electron emission in low energy ion-atom collisions [22,23] and photoionization close to threshold [24].

### 1.1.2 Reaction Microscopes: Magnetic Guiding of Electrons

To circumvent the limitations associated with direct imaging and to increase the electron energy acceptance for $4\pi$ collection maintaining at the same time the full resolution in the recoil-ion branch novel spectrometers have been developed where a solenoidal magnetic field parallel to the electric field is superimposed [25]. This magnetic field acts over the whole flight-path and it forces electrons to move on spiral trajectories from the reaction volume to the detector. In practice the magnetic field is generated by a pair of large Helmholtz coils placed outside of the vacuum-chamber (Fig. 1.8). Typical coil diameters range from 50 cm up to 2 m depending on the geometrical extension of the electron flight path. In order to avoid field distortions no magnetic materials and ideally only those with a small magnetic susceptibility

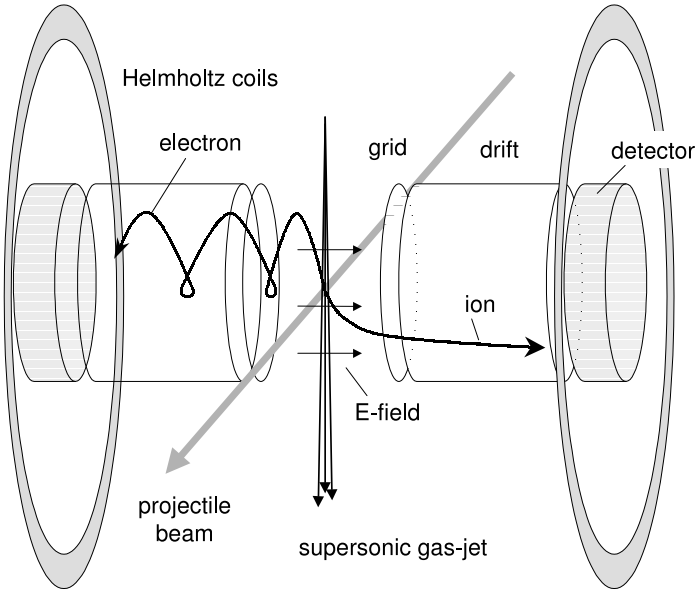


**Fig. 1.8.** Schematics of an reaction microscope.

should be used for construction of an reaction-microscope. A schematic setup is shown in Fig. 1.8. It basically consists of an electric extraction field with two subsequent drift paths and position sensitive detectors on either side. The extraction field is generated by means of potential rings in connection with an voltage divider or between two ceramic plates covered with an resistive layer [25]. The target point is defined by the cross-over of supersonic gas jet and particle beam.

Though the electron motion is strongly modified by the magnetic field it is still possible to reconstruct both, the electron trajectory and initial momentum vector from the two position informations and the measured time-of-flight. For a homogeneous magnetic field parallel to the electric extraction field, the longitudinal (i.e. along the TOF-direction) motion of a charged particle is not changed (Eq. (1.1)) is still valid). In the transverse direction (perpendicular to the field axis), however, the electron travels along a circle with radius $R = P_\perp/(qB)$ where the time $T$ for one turn is given by the inverse of the cyclotron frequency $\omega = q \cdot B/m = 2\pi/T$, with $B$ being the magnetic field strength, $m$ and $q$ the electron mass and charge, respectively. In useful units these equations are

$$\omega = 9.65 \cdot 10^{-6} \cdot qB/m \qquad \text{and} \qquad R = 12.39 \cdot p_\perp/qB\,, \tag{1.14}$$

with $\omega$ in nsec$^{-1}$, $q$ and $p$ in atomic units, $B$ in Gauss and $m$ in amu. With a magnetic field of only 10 G, all trajectories of electrons with energies up to 100 eV are confined to a cylinder with a radius of 3.3 cm, independent

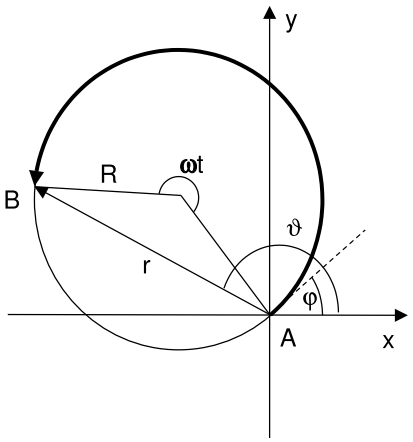


**Fig. 1.9.** Projection of an electron trajectory onto the detector surface. The magnetic field is perpendicular to the paper-plane (see text).

of the electric field strength and independent of the spectrometer geometry. Hence, a electron detector with 8 cm diameter is sufficient to achieve a $4\pi$ collection efficiency for electron energies of more than 100 eV. Under these conditions the revolution time for electrons is 35 ns and more than 250 $\mu$s for He ions. Thus, it is in the range or even smaller than typical electron flight-times. On the other hand, the cyclotron time for ions is much longer than usual ion flight-times indicating that their trajectories are only weakly affected by the magnetic field. It basically results in a slight rotation of the ion image on the recoil detector. In most cases it is sufficient to compensate this by rotating the whole ion position distribution by the corresponding angle. In conclusion, by changing the magnetic field strength the accepted maximum transverse momentum of electrons is adjustable without affecting the recoil-ion imaging. It is essentially this electron zooming option which makes reaction microscopes extremely versatile and which considerably extended the range of applications for coincident electron-ion imaging (see also [2]).

### 1.1.3 Reconstruction of Electron Momenta

Below we discuss how to calculate the initial electron momentum components from the position and time information. Whereas the longitudinal electron momentum solely and unambiguously follows from the TOF, both, position and time are required to reconstruct the two transverse momentum components. To illustrate this we consider the projection of an electron trajectory onto the electron detector surface, i.e. onto a plane perpendicular to the magnetic field axis (Fig. 1.9). The electron is emitted with a transverse momentum $p_\perp$ at the origin (point A) under a certain angle $\varphi$ with respect to

the positive $x$-axis. On its way to the electron detector it travels on a spiral trajectory, i.e. along a circle, before it hits the detector at B with a certain displacement $r$. For a given magnetic field the radius $R$ of the cyclotron motion is a direct measure of $p_\perp$ (see Eq. 1.14) while the arc-angle $\omega t$ depends only on the electron time-of-flight. From simple geometrical considerations (Fig. 1.9) follows that

$$R = \frac{r}{2|\sin(\omega t/2)|} \tag{1.15}$$

Thus, the magnitude of the transverse momentum $p_\perp$ can be calculated from the position of detection, $(r, \vartheta)$ in cylindrical coordinates, and the measured electron TOF $t$ using the equations 1.14 and 1.15. With the initial angle of emission $\varphi$, which follows immediately from

$$\varphi = \vartheta - \omega t/2 \tag{1.16}$$

all three components of the electron momentum vector are determined.

Up to now we restricted the discussion to cases where the electron TOF is shorter than the cyclotron time or, in other words, where the electron passes through less than one complete turn. In many practical situations, however, the electrons perform several full turns $N$ (up to ten) of the cyclotron motion. If this happens then $\omega t$ has to be replaced by $\omega t - N \cdot 2\pi$ where $N$ is the next lowest integer of the ratio $(\omega t)/(2\pi)$. But still, the assignment of measured quantities and initial momentum is unique, as long as the denominator in Eq. 1.15 is larger than zero. The only prerequisite for reconstruction is the knowledge of the magnetic field strength and direction, respectively. Whenever electrons perform exactly one or several complete turns they hit the detector at the origin (point A in Fig. 1.9) independent of their initial transverse momentum or, in other words, all electrons with flight times equal to a multiple integer of $T$ (the inverse cyclotron frequency) are focussed onto the same spot on the detector and no momentum information is obtained. These specific cases appear as nodal points when the radial displacement on the electron detector is plotted versus the electron time-of-flight (Fig. 1.10). Though the momentum information is lost at these nodes, however, they deliver important and valuable information. First they serve as a good control of the experimental conditions and, more important, they allow a very precise and intrinsic determination of the magnetic field via a measurement of the inverse cyclotron frequency. It is given by the time-distance of two nodes. Whenever important information about the physical process is masked by these nodes, which might happen, the magnetic field can be changed slightly resulting in a corresponding time-shift of the nodal points.

For a certain electron TOF the radial displacement $r$ on the detector is proportional to the transverse momentum. Thus, the momentum resolution in the transverse direction is given by $\Delta P_\perp = P_\perp \cdot \Delta r/r$ where $\Delta r$ is the effective position uncertainty resulting from both, the detector resolution and the target size. For an effective position resolution of 1 mm the transverse

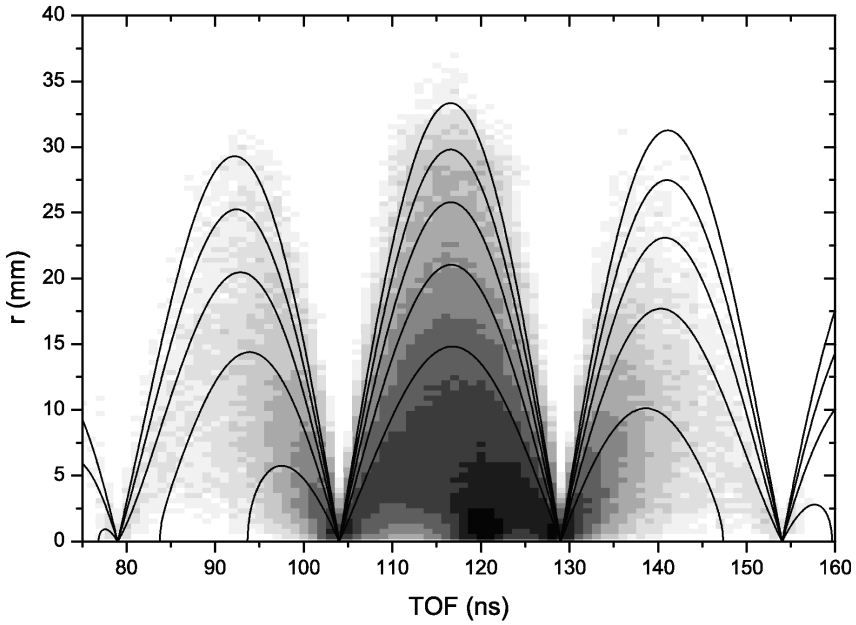


**Fig. 1.10.** The radial displacement $r$ of electrons on the detector versus their time-of-flight for single ionization of $H_2$ by 6 MeV proton impact. The magnetic field is about 14 G corresponding to a cyclotron revolution time of $T = 25$ ns. The solid lines are the calculated position and time dependences for isotropically emitted electrons with kinetic energies between 10 and 50 eV in steps of 10 eV. The point (TOF = 120 ns, $r = 0$) corresponds to the origin ($E = 0$) on the electron energy scale.

momentum of an electron which hits the detector at $r = 4$ cm with $p_\perp = 1$ a.u. is determined with an uncertainty of $\Delta P_\perp = 0.025$ a.u.. This value should be regarded as a lower limit because a finite time resolution, which enters into the determination of the sin-term in Eq. (1.15), as well as magnetic field distortions contribute in addition. As a consequence, a definite determination of the electron momentum resolution is hard to perform. For practical purposes and if high resolution is required, it is the best to check the actual resolution by using electrons with a well defined and sharp kinetic energy arising from known atomic processes like, e.g., Auger-electron emission or single photoionization.

### 1.1.4 New Developments

In this Chapter, a few technical developments related to recoil-ion and electron momentum spectroscopy, which are still ongoing and which might play a certain role in future applications, are listed and briefly discussed. Though

this list is quite incomplete it stands for a still continuing evolution of many-particle imaging devices to investigate atomic and molecular reactions.

To some extend, the limited number of target species accessible to COLTRIMS is a constraint. This is mainly because both conditions – high target density and extremely low temperature – are hard to combine if one thinks on targets like for example highly excited atoms, metastable helium, atomic hydrogen, positronium, vibrationally cold molecules or others. Very recently, the Frankfurt group succeeded in producing a supersonic jet of dense and internally cold metastable He atoms [26]. A high pressure discharge burning between the entrance and exit surface of a 50 $\mu$m nozzle collisionally excites He while the following adiabatic expansion into the vacuum reduces the internal temperature. After a subsequent Stern-Gerlach magnet the beam can be used for experiments with oriented and cold metastable helium atoms.

If complex targets are used, for example, molecules or clusters, the number of particles ejected from a break-up reaction can be quite large. The desire to detect all of them increases the demands on the detectors concerning their multi-hit capability. The hexagonal delay-line for position encoding fulfills the requirement of almost negligible dead-time as long as channel-plates with small or medium diameters are used. With increasing detector sizes the cable length and therewith the dispersion of signals traveling along the cables is increasing resulting in a slowing down of the detector read-out. On the other hand, with on-going development of integrated electronic circuits concerning speed and compactness large area pixel anodes with ultra-fast readout of individual pixels are in the realm of possibility. Presently, work is in progress to develop such an anode where one thousand or more pixels are individually read out using highly integrated electronics mounted on-board directly at the anode. It is hoped, that in the near future large active area detectors with improved multi-hit capability and high position resolution will be at hand.

The flexibility of imaging spectrometers can be increased further if the traditional concept of using only static electric and magnetic fields for projection and guiding of charged particles is skipped. Obviously, the application of pulsed or otherwise time-dependent fields can help to adapt the spectrometer performance to specific problems. To study for example molecular fragmentation maintaining at the same time a high resolution for the emitted electrons a pulsed extraction field can be used. The initially small field is ramped up considerably on a sub-$\mu$s time-scale whenever an electron hits the detector. Because even eV ions do not travel over a large distance in the time the electrons require to reach the detector. Thus, ionic fragments experience the large acceleration field ensuring a $4\pi$ detection efficiency for them. This method has been successfully applied the first time to investigate double photoionization of molecular hydrogen [27]. But, it is applicable for a large range of molecular break-up reactions and in most cases it is advantageous compared to a static field extraction.

An electric field between two grids placed at an appropriate position in the ion or electron flight-path can serve as a switchable potential barrier. By gating the applied voltage in synchronization with an external time reference, like the timing signal of an projectile detector, specific user defined parts of either the electron or the recoil-ion TOF spectrum can be masked out. Such kind of gated switches in the recoil-ion branch have been used to investigate electron transfer reactions in fast proton-helium collisions [28]. The huge amount of recoil-ions from unwanted physical reactions, which would overload the detector, could be effectively suppressed by many orders of magnitude. Recently, a similar technique has been used for high-resolution electron capture measurements. There the recoil-ions have been extracted exactly parallel to the incoming beam direction. A pulsed electric field acting perpendicular to the ion trajectory within the drift path kicked the recoil-ions onto the detector, which was mounted beneath the projectile beam axis [29]. This are only two examples where gated switches or deflectors have been used. In general, the possibilities opened up with pulsed electric fields are by far not yet exhausted.

## References

1. C.L. Cocke, R.E. Olson: Phys. Rep. **205**, 155 (1991)
2. J. Ullrich, R. Moshammer, R. Dörner, O. Jagutzki, V. Mergel, H. Schmidt-Böcking, L. Spielberger: J. Phys. B **30**, 2917 (1997)
3. R. Dörner, V. Mergel, O. Jagutzki, L. Spielberger, J. Ullrich, R. Moshammer, H. Schmidt-Böcking: Phys. Rep. **330**, 96 (2000)
4. J. Ullrich, H. Schmidt-Böcking: Phys. Lett. A **125**, 193 (1987)
5. R. Ali, V. Frohne, C.L. Cocke, M. Stöckli, S. Cheng, M.L.A. Raphaelian: Phys. Rev. Lett. **69**, 2491 (1992)
6. W.C. Wiley, I.H. McLaren: Rev. Sci. Instr. **26**, 1150 (1955)
7. R. Dörner, H. Bräuning, J.M. Feagin, V. Mergel, O. Jagutzki, L. Spielberger, T. Vogt, H. Khemliche, M.H. Prior, J. Ullrich, C.L. Cocke, H. Schmidt-Böcking: Phys. Rev. **A 57**, 1074(1998)
8. M.A. Abdallah, W. Wolff, H.E. Wolff, E.Y. Kamber, M. Stöckli, C.L. Cocke: Phys. Rev. **A 58**, 2911 (1998)
9. R. Miller, in: Atomic and Molecular Beam Methods, Vol. **14**, eds. G. Scoles, D. Bassi, U. Buck, D. Laine, Oxford University Press, New York, 1988
10. D. Fischer: Diploma Thesis, University Freiburg (2000)
11. S. Wolf, H. Helm: Phys. Rev. A **62**, 043408 (2000)
12. M. van der Poel, C. V. Nielsen, M.A. Gearba, N. Andersen: Phys. Rev. Lett. **87**, 123201 (2001)
13. J. W. Turkstra, R. Hoekstra, S. Knoop, D. Meyer, R. Morgenstern, R. E. Olson: Phys. Rev. Lett. 123202 (2001)
14. X. Flechard, H. Nguyen, E. Wells, I. Ben-Itzhak, B. D. DePaola: Phys. Rev. Lett. 123203 (2001)
15. B. DePaola et al.: Proceedings HCI 2002 (to be published in Nucl. Instr. and Meth. B)
16. A. Martin, P. Jenlinsky, M. Lampton, R.F. Malina: Rev, Sci. Instr. **52**, 1067 (1981)

17. S.E. Sobottka, M.B. Williams: IEEE Trans. Nucl. Sci. **35**, 348 (1988)
18. G. Battistone, P. Campa, V. Chiarella, U. Denni, E. Iarocci, G. Nicoletti: Nucl. Instr. and Meth. **202**, 459 (1982)
19. I. Ali, R. Dörner, O. Jagutzki, S. Nüttgens, V. Mergel, L. Spielberger, Kh. Khayyat, T. Vogt, H. Bräuning, K. Ullmann, R. Moshammer, J. Ullrich, S. Hagmann, K.-O. Groeneveld, C.L. Cocke, H. Schmidt-Böcking: Nucl. Instr. and Meth. B **149**, 490 (1999)
20. O. Jagutzki, A. Cerezo, A. Czasch, R. Dörner, M. Hattaß, M. Huang, V. Mergel, U. Spillmann, K. Ullmann-Pfleger, T. Weber, H. Schmidt-Böcking, G. Smith: IEEE Conference Proceedings (NSS), San Diego (2002), to appear
21. M. Schulz, R. Moshammer, W. Schmitt, H. Kollmus, R. Mann, S. Hagmann, R.E. Olson, J. Ullrich: Phys. Rev. A **61**, 2270 (2000)
22. R. Dörner, H. Khemliche, M.H. Prior, C.L. Cocke, J.A. Gary, R.E. Olson, V. Mergel, J. Ullrich, H. Schmidt-Böcking: Phys. Rev. Lett. **77**, 4520 (1996)
23. E Edgü-Fry, C L Cocke, E Sidky, C D Lin, M Abdallah, J. Phys. B **35**, 2603 (2002)
24. R. Dörner, J.M. Feagin, C.L. Cocke, H. Bräuning, O. Jagutzki, M. Jung, E.P. Kanter, H. Khemliche, S. Kravis, V. Mergel, M.H. Prior, H. Schmidt-Böcking, L. Spielberger, J. Ullrich, M. Unverzagt, T. Vogt: Phys. Rev. Lett. **77**, 1024 (1996)
25. R. Moshammer, M. Unverzagt, W. Schmitt, J. Ullrich, H. Schmidt-Böcking: Nucl. Instr. and Meth. B **108**, 425 (1996)
26. T. Jahnke et al.: http://hsbpc1.ikf.physik.uni-frankfurt.de/plasmajet/plasmajet.html
27. R. Dörner, H. Bräuning, O. Jagutzki, V. Mergel, M. Achler, R. Moshammer, J.M. Feagin, T. Osipov, A. Bräuning-Demian, L. Spielberger, J.H. McGuire, M.H. Prior, N. Berrah, J.D. Bozek, C.L. Cocke, H. Schmidt-Böcking: Phys. Rev. Lett. **81** 5776 (1998)
28. H. T. Schmidt, A. Fardi, R. Schuch, S. H. Schwartz, H. Zettergren, and H. Cederquist, L. Bagge, H. Danared, A. Källberg, J. Jensen, and K.-G. Rensfelt, V. Mergel, L. Schmidt, and H. Schmidt-Böcking, C. L. Cocke: Phys. Rev. Lett. **89**, 163201 (2002)
29. D. Fischer, B. Feuerstein, R.D. DuBois, R. Moshammer, J.R. Crespo Lopez-Urrutia, I. Draganic, H. Lörch, A.N. Perumal, J. Ullrich: J. Phys. B **35** 1369 (2002)